Formation of amorphous Al_2O_3 phase on aluminum alloy by *in-situ* laser cladding

T. M. YUE, K. J. HUANG, H. C. MAN
The Advanced Manufacturing Technology Research Centre, Department of Industrial and Systems Engineering, The Hong Kong Polytechnic University, Hung Hom, Hong Kong

It is well known that amorphous materials have excellent mechanical, physical and chemical properties, and thus, synthesizing an amorphous layer on crystalline substrates can significantly improve the surface performances of the substrate material. Surface amorphization can be achieved by laser surface treatment due to the rapid heating and cooling characteristics of laser treatment, which inhibit long-range diffusion and prevent crystallization. Amorphous layers and amorphous-crystalline coexisting layers have been obtained by various laser surface treatment techniques, such as the laser direct remelting of substrate materials [1, 2]; laser remelting of plasma-sprayed coatings [3]; laser remelting of laser-clad coatings [4]; laser alloying [5]; laser cladding of high glass-forming ability powders [6] and laser-induced self-propagating reactions [7]. The present paper describes the synthesis of the Al_2O_3 amorphous phase on aluminum alloy 7075 by the method of *in-situ* laser cladding through the thermite reaction between CuO and Al powders.

The mixed powders of CuO(3 mol) + Al(2 mol) + SiO_2(3 mol) were pre-placed on an Al-7075 alloy substrate using a pasting binder. The nominal mesh size of the powders was 200, which is equivalent to a particle size of 70 μm; the thickness of pre-placement was approximately 0.5 mm. A high-power PRC CW-CO_2 laser was employed for track melting under an Ar-shielding atmosphere. The diameter of the laser spot and the laser power were kept constant at 2 mm and 1800 W, respectively; whereas a laser-scanning velocity of 25 mm/s, and a 50% track-overlapping condition were used. The substrate was water-cooled during the laser cladding. SiO_2 powders were used to slow down the exothermic reaction, since it was found that a mole ratio of 2Al:3CuO would result in violent reactions.

The different phases of the clad layer were determined with an X-ray diffraction technique using Cu-K_α radiation at 40 KV and 30 mA (Philips PW-3710), energy dispersive X-ray spectroscopy (EDX) and transmission electron microscopy (Jeol 2010). Cross-sectional specimens were prepared for the TEM and high-resolution TEM study (HRTEM). The TEM specimens were mechanically ground and polished to a thickness of about 30 μm. This was followed by ion milling, which used Ar^+ bombardment at 5 keV using a Gatan Precision Polishing System.

Fig. 1 shows a typical microstructure of the clad layer, which clearly shows two distinct zones: the Al_2O_3 reaction layer (R) and the fusion layer (F). Fig. 2 shows the XRD results of the clad layer, which show that the α-Al_2O_3, γ-Al_2O_3, Al_2Cu and Cu_2O phases are present in the laser-processed zone.

At the top of the Al_2O_3 reaction layer (Fig. 3), a complete amorphous structure of Al_2O_3 phase is present (labelled A); underneath it, a structure consisting of an amorphous Al_2O_3 phase and fine crystallines of γ-Al_2O_3 (labelled B) is found. This is followed by a structure composed of a metastable γ-Al_2O_3 phase (labelled C). The compositions of the various phases found in locations A, B, and C are present in Table I. The outermost layer of the reaction zone is confirmed to have an amorphous structure based on the broadened halo configurations of the selected-area electron diffraction (SAED) patterns (Fig. 4) and the lattice image of amorphous structures (Fig. 5). The XRD results did not show any obvious peaks for the amorphous phase. This could be due to the amount of the phase which is below the detection limit of the technique. The SAED pattern for structure B consists of broadened halos and diffraction spots from [001] of the γ-Al_2O_3 phase (Fig. 6). The SAED pattern for the metastable γ-Al_2O_3 phase of structure C is shown in Fig. 7, a dark field image of which is shown in Fig. 8. It is estimated that the thickness of the amorphous Al_2O_3 zone is about 500 nm, while the thickness of zone B is some 50–150 nm, and the size of the γ-Al_2O_3 crystallines is about 600 nm.

It is well known that glass forming ability is governed by the chemical composition of the molten pool and the cooling rate of the melts. In the present study, the formation of the amorphous Al_2O_3 phase is considered to be due to the high cooling rate of the Al_2O_3 melt and to the presence of the reduced metalloid Si. The mechanism of *in-situ* laser cladding is highly complex, especially when thermite reactions are involved. Nonetheless, an estimation of the cooling rates, $\partial T/\partial t$, for *in-situ* laser cladding at high scanning speeds can be made using the Rosenthal solution for a moving heat point source [4]:

$$\partial T/\partial t = -2\pi\kappa \times (V/P) \times (\Delta T)^2 \qquad (1)$$

where κ is the thermal conductivity, V is the scanning speed, P is the absorbed laser power which is equal to $P_{\text{total}}(1 - R)$, R is the fraction of reflection, and ΔT is the range of temperature variation during cooling. In the calculation, it is assumed that the maximum temperature in the clad pool is lower than that of the boiling temperature of Al_2O_3, and is higher than that of

0022–2461

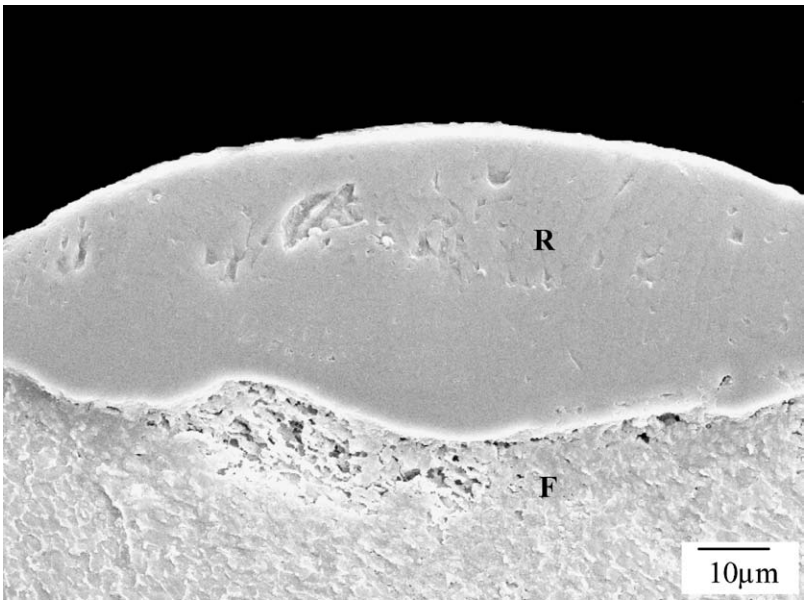

Figure 1 An SEM photo showing the Al_2O_3 reaction layer (R) and the fusion layer (F) (etched in Keller's reagent).

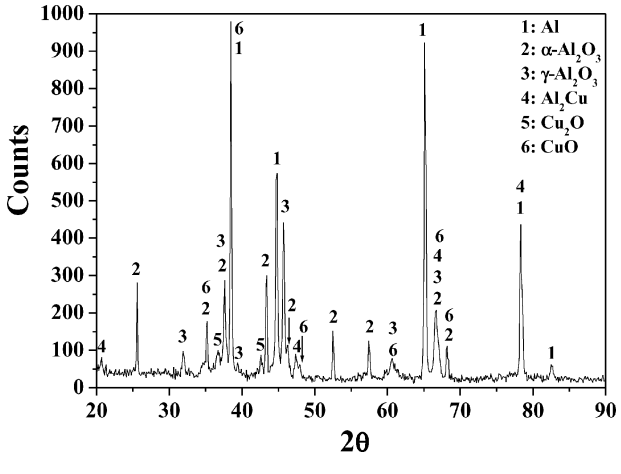

Figure 2 The XRD results of the clad layer.

TABLE I The EDX results for locations A, B and C

Location	Al (at.%)	O (at.%)
A	46.78	53.22
B	33.70	66.30
C	43.92	56.08

the melting temperature of Al_2O_3, given the realization that the heat generated by the thermite reaction of $3CuO + 2Al \rightarrow Al_2O_3 + 3Cu$ is high enough to heat up the reaction products of 3 mol Cu and 1 mol Al_2O_3 from the reaction temperature (1133 K) to the melting temperature of Al_2O_3 (2327 K). Table II presents the results of the calculated cooling rates for Al_2O_3 under the laser cladding condition of this study. The

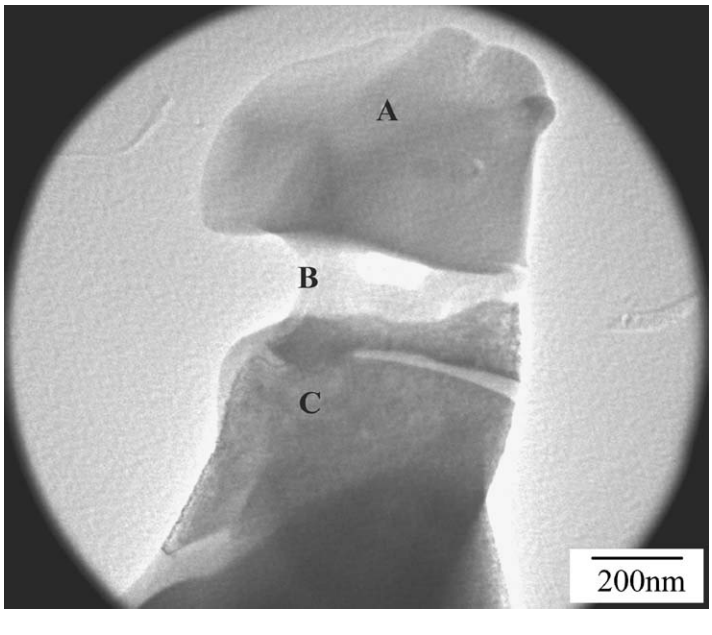

Figure 3 A TEM bright field image of the top surface of the reaction layer.

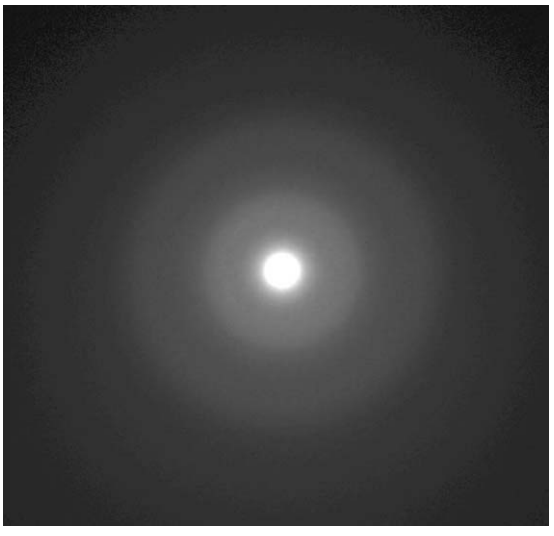

Figure 4 The diffraction pattern of the amorphous Al_2O_3 phase at location A in Fig. 3.

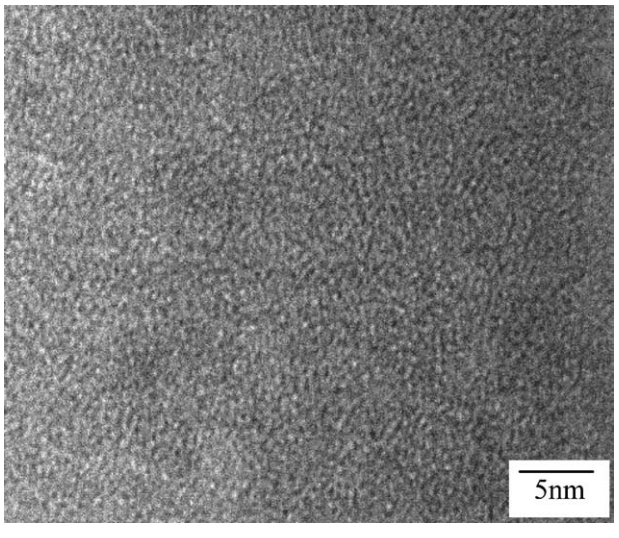

Figure 5 A high-resolution TEM image of the structure at location A.

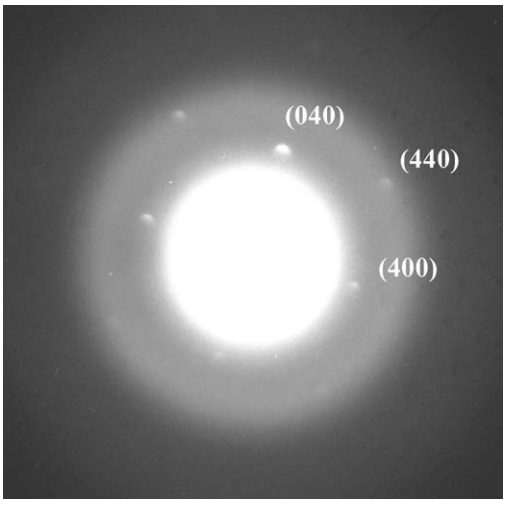

Figure 6 The diffraction pattern of the amorphous Al_2O_3 phase coexisting with crystallines of γ-Al_2O_3 at location B.

results show that the cooling rate of the Al_2O_3 phase is in the order of 10^3–10^4K/s, which is similar to that obtained by other studies on laser surface treatments [2, 8]. This cooling rate is believed to be high enough

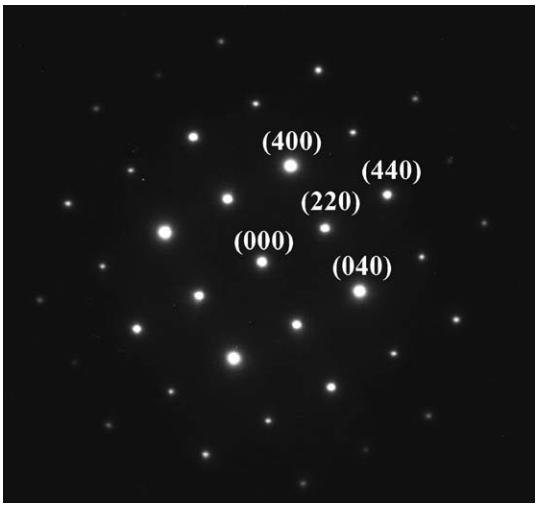

Figure 7 The electron diffraction pattern from [001] of the γ-Al_2O_3 phase at location C.

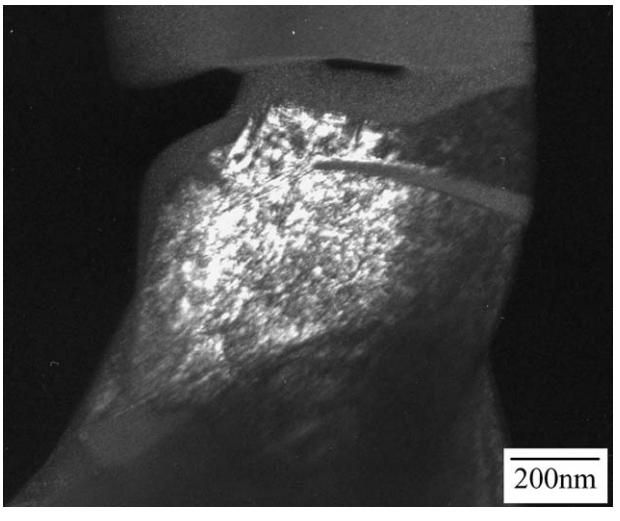

Figure 8 A dark field image of spot (040) shown in Fig. 7.

to allow the metastable γ-Al_2O_3 phase to form, since it was reported that a cooling rate in the order of 400 K/s is enough to form the γ-Al_2O_3 phase [9]. Moreover, Cao [10] believed that if the cooling rate was high enough, the long-range order of the γ-Al_2O_3 phase could break up entirely and an amorphous Al_2O_3 structure could be produced. In fact, during the solidification of the laser melt pool, the temperature gradient (G) at the solidification front will steadily decrease from the bottom of the melt to the top surface, and the solidification rate (V) of the melt-liquid interface will increase from zero at the bottom to a maximum at the top surface. That means that the cooling rate (R) will increase from the bottom of the melt to the top surface of the clad layer according to the relationship of $R = GV$. In other words, the top surface layer will experience the highest cooling rate

TABLE II The laser parameters and the calculated cooling rates

P (W)	1080
V (m/s)	0.025
κ (W/m · K) [16]	7.1128–25.104
ΔT (K)	2029
$-\partial T/\partial t$ (K/s)	4.26×10^3–1.5×10^4

and, as a result, an amorphous Al_2O_3 phase could form at the outermost surface of the Al_2O_3 reaction layer.

However, a fast cooling rate alone may not be good enough for the amorphous Al_2O_3 phase to form under the conditions of this study. A parallel study shows that when the laser cladding experiment was performed without SiO_2 powders, no amorphous phase was detected. It is considered that when SiO_2 powders are present in the pre-mixed cladding powders, they can react with the molten aluminum. When the pre-placed powder mix, which is composed of SiO_2, is irradiated by the laser light, a thermite reaction between CuO and Al powders is initiated when the temperature is raised to about 1133 K [11],

$$3CuO + 2Al \rightarrow Al_2O_3 + 3Cu. \quad (2)$$

Notwithstanding the short interaction time between the laser light and the coating, it is considered that the melting of the pre-placed coating started with the aluminum powders, which have a relatively low melting point. Therefore, apart from the above thermite reaction, SiO_2 can react with molten aluminum according to the following reaction: $3SiO_2 + 4Al \rightarrow 3Si + 2Al_2O_3$. As a result, silicon is produced. Previous studies have shown that silicon can improve the thermal stability of the supercooled liquid and enhance the glass-forming ability of some metallic glass-forming alloys [12, 13]. This was considered to be attributed to the neutralizing effect of nucleation sites by silicon. On the other hand, Li [14] believed that the addition of elements with small-sized atoms, such as C, B and Si, can increase the degree of disorder of the atoms in glass-forming alloys, and consequently improve the amorphous forming ability of the alloy. In the present study, the exact role of silicon in promoting the formation of the amorphous Al_2O_3 phase is still unclear, and further research is required. It should be pointed out that no silicon was detected by the energy disperse X-ray (EDX) analysis within the locations of A, B, and C. This could be because the amount present was below the detection limit. The limits of solubility of silicon in Al_2O_3 are 220 and 300 ppm at 1773 and 1873 K, respectively [15].

Acknowledgments

This work was fully supported by the Research Grants Council of the Hong Kong Special Administrative Region, China (Project no. PolyU5194/02E). The authors are grateful to Dr G. K. H. Pang of the Department of Applied Physics for his assistance in performing the TEM work. The infra-structural support provided by PolyU is also acknowledged.

References

1. D. G. MORRIS, *Mater. Sci. and Engng.* **97** (1988) 177.
2. J. G. ZHANG, X. M. ZHANG, Y. T. LIN and K. JUN, *J. Mater. Sci.* **23**(12) (1988) 4357.
3. G. Y. LIANG and T. T. WONG, *Surf. Coat. Techn.* **89**(1–2) (1997) 121.
4. F. AUDEBERT, R. COLACO, R. VILAR and H. SIRKIN, *Scripta Materialia* **48**(3) (2003) 281.
5. X. L. WU and Y. S. HONG, *Metall. Mater. Trans.* A **31A**(12) (2000) 3123.
6. X. L. WU, B. XU and Y. S. HONG, *Mater. Lett.* **56**(5) (2002) 838.
7. C. S. WANG, L. H. GAO, G. LI, Y. F. WANG, Y. L. XIA, C. DONG and S. BYSAKH, *J. Mater. Sci.* **38**(7) (2003) 1377.
8. W. AZZOLINI, M. C. F. IERARDI, A. GARCIA and R. VILAR, *Lasers in Engineering* **9**(3) (1999) 229.
9. J. A. VREELING, Y. T. PEI, B. WIND, V. OCELÍK and J. TH. M. DE HOSSON, *Scripta Materialia* **44**(4) (2001) 643.
10. S. CAO, A. J. PEDRAZA, D. H. LOWNDES and L. F. ALLARD, *Appl. Phys. Lett.* **65**(23) (1994) 2940.
11. G. CHEN, G. X. SUN and Z. G. ZHU, *Mater. Sci. and Engng.* A **A251**(1–2) (1998) 226.
12. H. CHOI-YIM, R. BUSCH and W. L. JOHNSON, *J. Appl. Phys.* **83**(12) (1998) 7993.
13. C. A. VOLKERT, PhD Thesis, Harvard University, 1988.
14. G. LI, Y. Q. XIA, Y. F. WANG, C. S. WANG, Y. L. XIA, C. DONG and J. J. LU, *Tribology* **22**(5) (2002) 343.
15. A. KEBBEDE and A. H. CARIM, *Mater. Lett.* **41**(4) (1999) 198.
16. J. F. SHACKELFORD and W. ALEXANDER, in "CRC Materials Science and Engineering Handbook," 3rd ed. (CRC Press LLC, 2000) p. 407.

Received 6 May
and accepted 20 May 2004